Supporting Information

Generation of Spin Defects by Ion Implantation in Hexagonal Boron Nitride

Nai-Jie Guo,[1,2] Wei Liu,[1,2,*] Zhi-Peng Li,[1,2] Yuan-Ze Yang,[1,2] Shang Yu,[1,2] Yu Meng,[1,2] Zhao-An Wang,[1,2] Xiao-Dong Zeng,[1,2] Fei-Fei Yan,[1,2] Qiang Li,[1,2] Jun-Feng Wang,[1,2] Jin-Shi Xu,[1,2] Yi-Tao Wang,[1,2,†] Jian-Shun Tang,[1,2,‡] Chuan-Feng Li,[1,2,§] and Guang-Can Guo[1,2]

[1]*CAS Key Laboratory of Quantum Information, University of Science and Technology of China, Hefei, P.R.China*

[2]*CAS Center For Excellence in Quantum Information and Quantum Physics, University of Science and Technology of China, Hefei, P.R.China*

(Dated: December 6, 2021)

Contents

This Supporting Information contains 9 pages and 6 figures.

*Electronic address: lw691225@ustc.edu.cn

†Electronic address: yitao@ustc.edu.cn

‡Electronic address: tjs@ustc.edu.cn

§Electronic address: cfli@ustc.edu.cn

S1. SPIN PROPERTIES

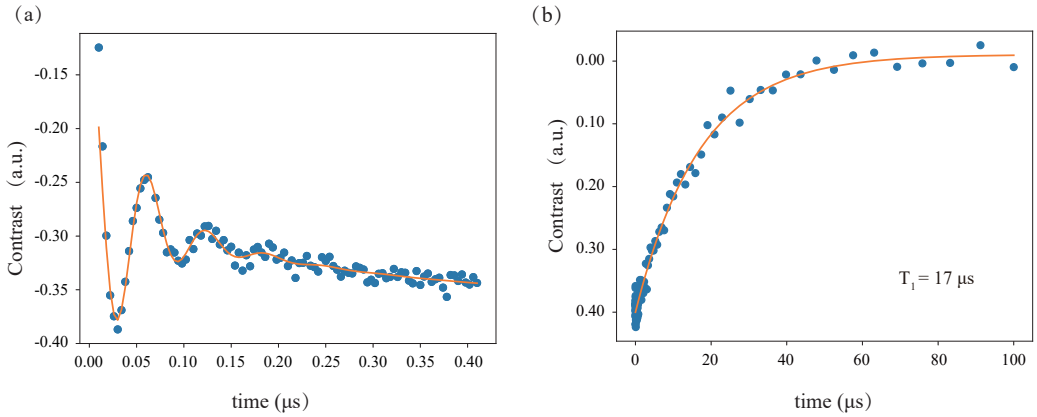

Figure S1. Spin properties of defects created by implanting helium ions with an energy of 30 keV and a fluence of 1×10^{14} ions/cm^2 without an external magnetic field. (a) Rabi oscillation of the defects. (b) A spin-lattice relaxation time of 17 μs at room temperature.

For the Rabi and T_1 experiment, we used a home-built confocal microscope combined with a microwave system [1, 2]. We measured the Rabi oscillation of the defects created by implanting helium ions with an energy of 30 keV and a fluence of 1×10^{14} ions/cm^2 without an external magnetic field, as shown in Figure S1(a). From the Rabi frequency, we obtained a spin-lattice relaxation time of 17 μs at room temperature, as shown in Figure S1(b).

S2. THE EFFECT OF IMPLANTATION PARAMETERS ON SPIN PROPERTIES

Some results for the effect of implantation parameters on spin properties are shown in Figure S2. Figure S2(a) shows that an implantation fluence ranging from 1×10^{13} to 1×10^{15} ions/cm^2 has little effect on the ZFS parameter D. Figure S2(b) shows that different ion species, such as helium, carbon, nitrogen and argon, have almost no effect on the ZFS parameter D. Figures S2(c) and (d) show that the ZFS parameters D and E both show obvious differences at different spots when the fluence reaches 1×10^{16} ions/cm^2. Figures S2(e) and (f) show that varying the implantation energy from 20 keV to 30 keV scarcely affects the ZFS parameters D or E. Figure S2(g) shows that the T_1 time changes little with the implantation energy.

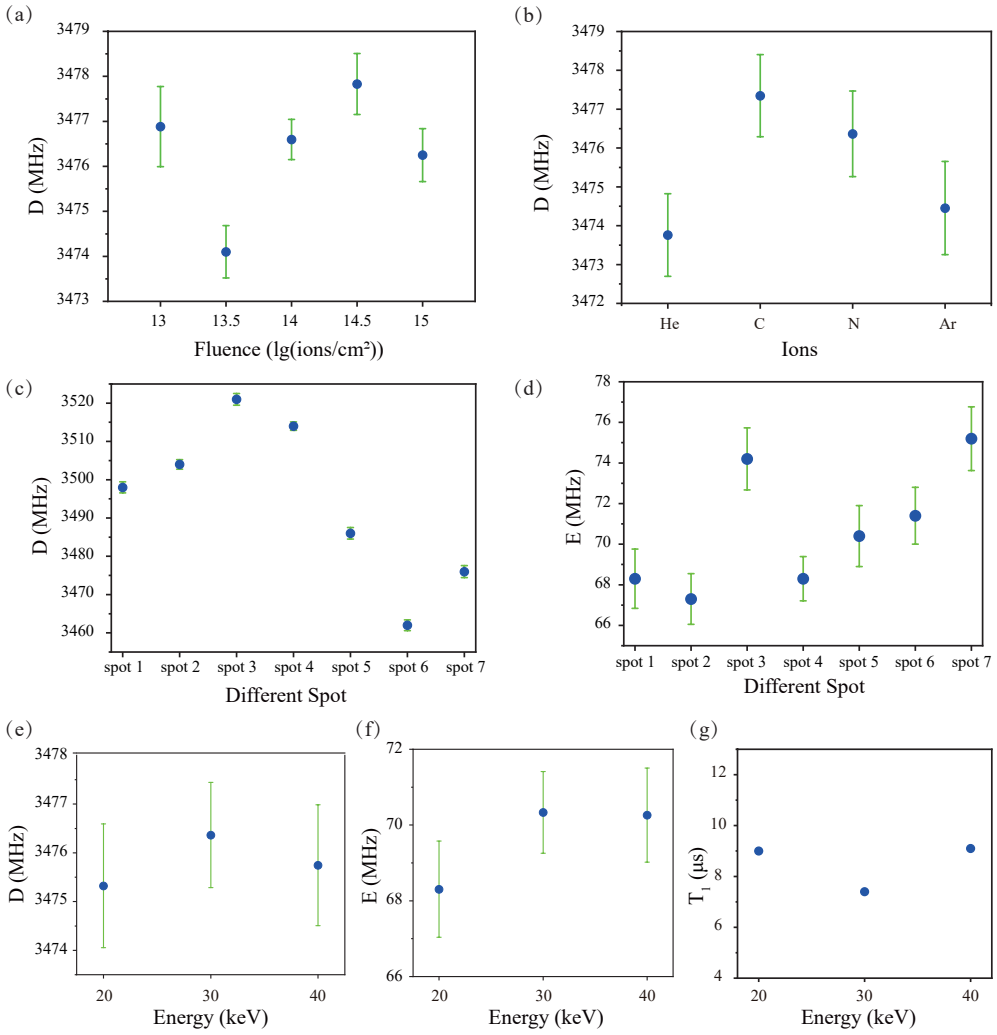

Figure S2. (a) The effect of the fluence on the ZFS parameter D. (b) The effect of different ion species on the ZFS parameter D. (c) The difference in the ZFS parameter D at different spots when the fluence reaches 1×10^{16} ions/cm^2. (d) The difference in the ZFS parameter E at different spots when the fluence reaches 1×10^{16} ions/cm^2. (e) The effect of the energy on the ZFS parameter D. (f) The effect of the energy on the ZFS parameter E. (g) The effect of the energy on the T_1 time.

S3. THE STABILITY AT ROOM TEMPERATURE

We measured the PL spectra under a 4.6-mW, 532-nm laser excitation over a period of 3 hours. A sample of V_B^- defects was created by implanting helium ions with an energy of 30 keV and a fluence of 1×10^{14} ions/cm^2. PL spectra as a function of time are shown

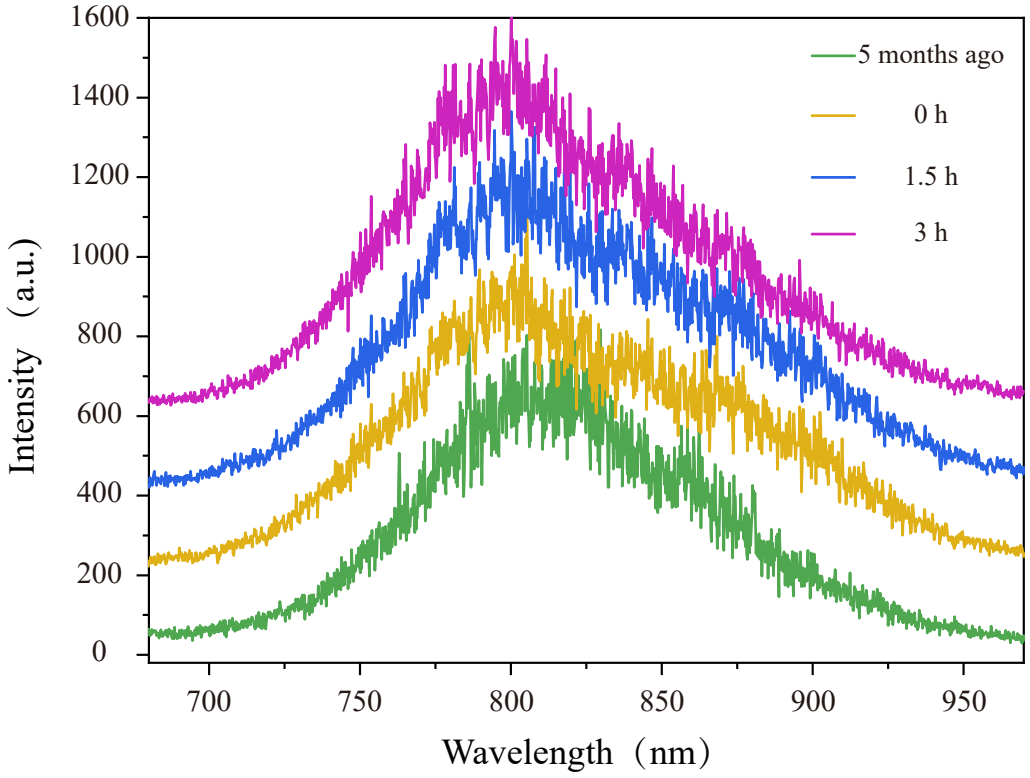

Figure S3. PL spectra as a function of time.

in Figure S3. The green line was measured five months previously. We can see that the V_B^- defects can be stored for a long time at room temperature and are stable under laser excitation, which exhibits good photostability at room temperature.

S4. HIGH-CONTRAST ODMR SPECTRA

The ODMR spectra measured by using gold electrode antenna to deliver a microwave field are shown in Figure S4. The ODMR contrast can reach up to 22% under high-power microwave (10 W) driving, and its two peaks overlap due to high power broadening, as shown in Figure S4(a). The ODMR contrast can readily reach approximately 13% without significant power broadening using low-power microwave (0.1 W) driving, as shown in Figure S4(b).

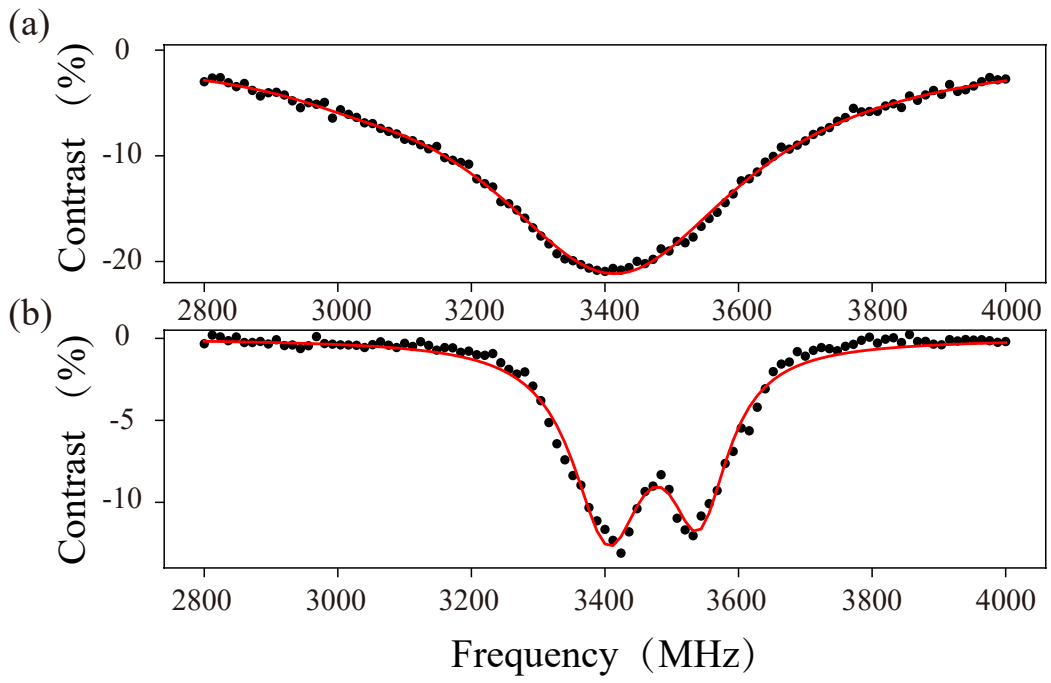

Figure S4. High-contrast ODMR spectra. (a) Measured ODMR spectrum under high-power microwave (10 W) driving. (b) Measured ODMR spectrum under low-power microwave (0.1 W) driving.

S5. THE PROBABILITY OF GENERATING A V_B^- CENTER PER ION

It is difficult to detect the exact number of V_B^- defects in an ensemble. However, we can approximately estimate the order of magnitude of the defect number from the photon count pumped by a pulsed laser (picosecond pulse width). Then, the probability of generating a V_B^- center per ion in the beam can also be estimated.

For the pulsed laser, each pulse can only be used to excite each defect once, and thus at most only one fluorescence photon can be emitted per defect. When the number of photons in one pulse exceeds the number of defects, we can simply assume that the fluorescence photon number is a lower bound for the defect number (considering the nonradiative transition, the fluorescence photon number should be less than the defect number).

By measuring the laser saturation curve (shown in Figure S5, our maximal laser power is 20 mW) we can obtain the saturation-excitation power (9.6 mW). We can assume that the number of photons per pulse exceeds the number of defects beyond the saturation power.

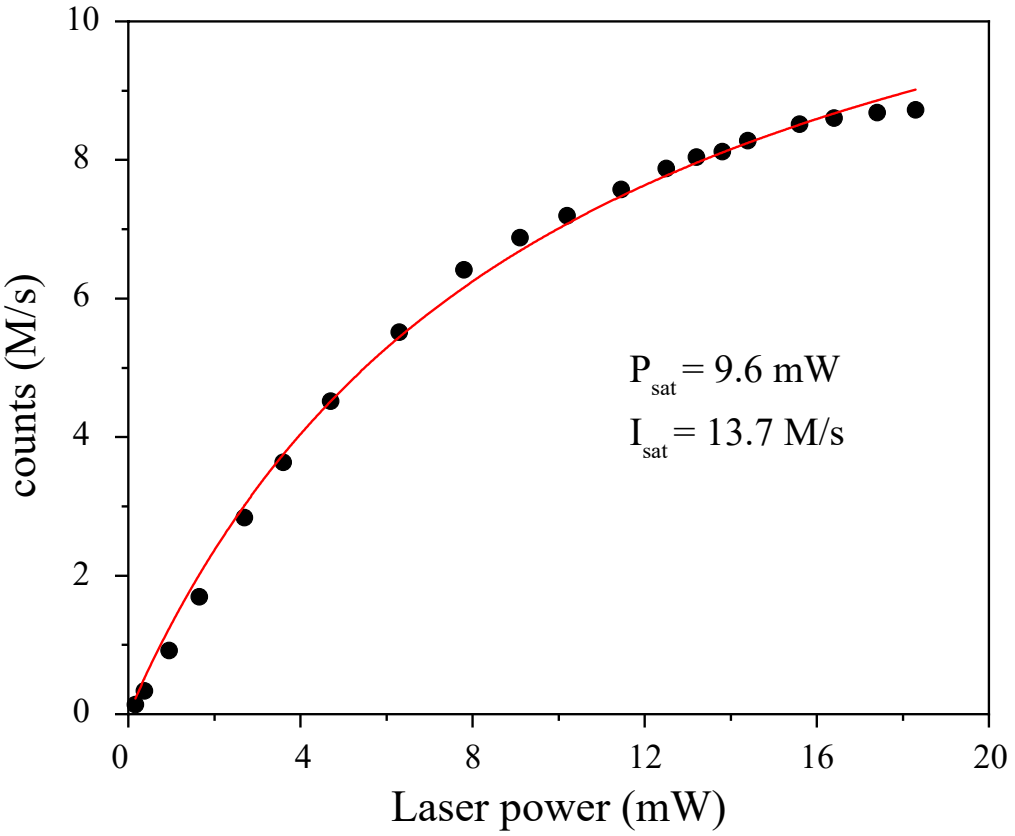

Figure S5. The laser saturation curve fitted by the function $I(P) = I_{sat}P/(P_{sat} + P)$, where I_{sat} and P_{sat} are the fitting parameters, and P is the excitation power. I_{sat} equals the saturation-radiation rate, and P_{sat} is the saturation-excitation power.

Considering the loss of fluorescence photons, we can estimate a lower bound for the generation probability by using the following equation,

$$Pro = \frac{\frac{I_{sat}}{\eta N}}{F * \pi * (\frac{0.61\lambda}{N.A.})^2}$$

where I_{sat} (13.7 M/s) is the saturated count, η ($\sim$0.8%) is the loss coefficient (including objective collection efficiency (28%) and coupling efficiency on the collection side (10%), filter and BS transmission efficiency (40%), and detection efficiency of single photon detector (70%)), N (78 M/s) is pulse number per second, F (10^{14} cm^{-2}) is implantation fluence, λ (532 nm) is the laser wavelength, and the N.A. is equal to 0.9. Therefore, the magnitude for the order of the lower bound of the generation probability was calculated to be $\sim 10^{-3}$%.

S6. A COMPLEMENT TO THE DEPENDENCE OF T_1 AND ION SPECIES

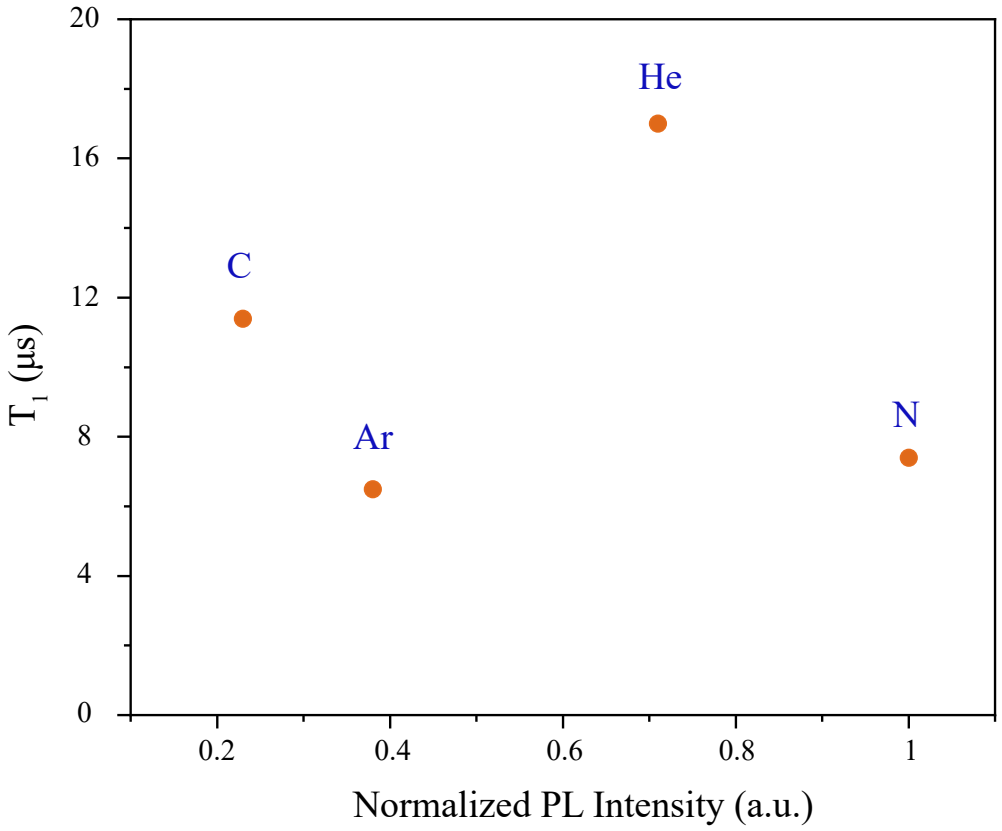

Figure S6. The dependence of T_1 and PL intensity when different ion species are used. The horizontal axis is the normalized PL intensity, and the vertical axis is the T_1 time.

According to our results, the T_1 time decreases as the ion radius increases. We speculate that with increasing ion radius, the damage increases due to the larger collision cross-section. For simplicity, we can regard crystal damage as defect density. We plotted the dependence of T_1 and normalized PL intensity when different ion species are used, as shown in Figure S6. It is difficult to discern an obvious dependence between the T_1 time and PL intensity. Nevertheless, we suspect that the T_1 time is related to defect density, because the PL intensity only represents the density of V_B^- defects. There is possibility that our bombardment is not only creating local defects but also removes several neighboring atoms and creates other defects [3, 4], especially when the damage is large enough. Therefore, although the damage increases with the increase of ion radius, the V_B^- defect density may not increase, but other

defect density may increase.

---

[1] Liu, W.; Li, Z.-P.; Yang, Y.-Z.; Yu, S.; Meng, Y.; Wang, Z.-A.; Guo, N.-J.; Yan, F.-F.; Li, Q.; Wang, J.-F.; Xu, J.-S.; Dong, Y.; Chen, X.-D.; Sun, F.-W.; Wang, Y.-T.; Tang, J.-S.; Li, C.-F.; Guo, G.-C. Rabi oscillation of V_B^- spin in hexagonal boron nitride. *ArXiv preprint arXiv:2101.11220* **2021**.

[2] Gottscholl, A.; Diez, M.; Soltamov, V.; Kasper, C.; Sperlich, A.; Kianinia, M.; Bradac, C.; Aharonovich, I.; Dyakonov, V. Room temperature coherent control of spin defects in hexagonal boron nitride. *Sci. Adv.* **2021**, 7, eabf3630.

[3] Jin, C.; Lin, F.; Suenaga, K.; Iijima, S. Fabrication of a Freestanding Boron Nitride Single Layer and Its Defect Assignments. *Phys. Rev. Lett.* **2009**, 102, 195505.

[4] Feng, J.; Deschout, H.; Caneva, S.; Hofmann, S.; Lončić, I.; Lazić, P.; Radenovic, A. Imaging of Optically Active Defects with Nanometer Resolution. *Nano Lett.* **2018**, 18, 1739–1744.